Understanding the Dynamics Behind the Photoisomerization of a Light-Driven Fluorene Molecular Rotary Motor

Andranik Kazaryan,[†] Jos C. M. Kistemaker,[‡] Lars V. Schäfer,[§] Wesley R. Browne,[‡] Ben L. Feringa,*[,‡] and Michael Filatov*[,†]

Theoretical Chemistry, Zernike Institute for Advanced Materials, University of Groningen, Nijenborgh 4, 9747 AG Groningen, Netherlands, Synthetic Organic Chemistry, Stratingh Institute for Chemistry, University of Groningen, Nijenborgh 4, 9747 AG Groningen, Netherlands, and Molecular Dynamics, Groningen Biomolecular Sciences and Biotechnology Institute, University of Groningen, Nijenborgh 4, 9747 AG Groningen, Netherlands

Received: January 21, 2010; Revised Manuscript Received: March 8, 2010

Light-driven molecular rotary motors derived from chiral overcrowded alkenes represent a broad class of compounds for which photochemical rearrangements lead to large scale motion of one part of the molecule with respect to another. It is this motion/change in molecular shape that is employed in many of their applications. A key group in this class are the molecular rotary motors that undergo unidirectional light-driven rotation about a double bond through a series of photochemical and thermal steps. In the present contribution we report a combined quantum chemical and molecular dynamics study of the mechanism of the rotational cycle of the fluorene-based molecular rotary motor 9-(2,4,7-trimethyl-2,3-dihydro-1H-inden-1-ylidene)-9H-fluorene (**1**). The potential energy surfaces of the ground and excited singlet states of **1** were calculated, and it was found that conical intersections play a central role in the mechanism of photo conversion between the stable conformer of **1** and its metastable conformer. Molecular dynamics simulations indicate that the average lifetime of the fluorene motor in the excited state is 1.40 ± 0.10 ps when starting from the stable conformer, which increases to 1.77 ± 0.13 ps for the reverse photoisomerization. These simulations indicate that the quantum yield of photoisomerization of the stable conformer is 0.92, whereas it is only 0.40 for the reverse photoisomerization. For the first time, a theoretical understanding of the experimentally observed photostationary state of **1** is reported that provides a detailed picture of the photoisomerization dynamics in overcrowded alkene-based molecular motor **1**. The analysis of the electronic structure of the fluorene molecular motor holds considerable implications for the design of molecular motors. Importantly, the role of pyramidalization and conical intersections offer new insight into the factors that dominate the photostationary state achieved in these systems.

Introduction

Light-driven changes in molecular structure represents one of the most important paradigms in the design of molecular machines and devices.[1−11] A wide range of molecular structures incorporating stilbene, azobenzene,[8] fulgides, diaryethenes,[10] etc. have been explored to achieve this level of functionality. Light-driven molecular rotary motors derived from chiral overcrowded alkenes[4,6,7,12−21] are a key class of compounds that utilize sequential photochemical and thermal rearrangements in their operation. The mode of action of these molecular motors is based on the periodic repetition of photoisomerization and thermal relaxation steps (see Scheme 1) that lead to unidirectional rotation of one part of the molecule (rotor) with respect to another (stator).[4,6,7,12] To date, empirical studies and judicious synthetic modifications have allowed for a very high degree of control over the thermal step limited rotation speed (ca. 10^8 times) through lowering of the activation energy of the thermal helix inversion.[13−15] The photoisomerization step, however, still remains poorly understood and less amenable to prediction with regard to the effect of synthetic modifications. The effect of various factors, such as substituents and heteroatoms introduced in the rotor and the stator parts,[16] the effect of environment,[22] on the dynamics of photorearrangement and on the geometric transformations that the motor undergoes, need to be considered to be able to improve the design of molecular motors.

SCHEME 1: Photochemical and Thermal Components of the Rotary Cycle of a Fluorene-Based Molecular Motor (1)

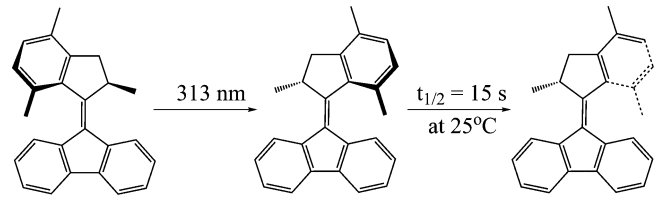

Here, we show that quantum chemical, molecular dynamics, and experimental data allow for an unprecedented understanding of the photoisomerization process. A theoretical investigation of the ground and excited state potential energy surfaces (PESs) of the molecular motor 9-(2,4,7-trimethyl-2,3-dihydro-1H-inden-1-ylidene)-9H-fluorene (**1**)[15] presents a first step

* To whom correspondence should be addressed: E-mail: b.l.feringa@rug.nl (B.L.F), m.filatov@rug.nl (M.F.).
[†] Zernike Institute for Advanced Materials.
[‡] Stratingh Institute for Chemistry.
[§] Groningen Biomolecular Sciences and Biotechnology Institute.

10.1021/jp100609m
Published on Web 03/29/2010

toward understanding the dynamics that lie at the heart of the rearrangements, both photochemical and thermal. In studying the photoisomerization, the key questions that will be addressed are: How important are conical intersections (CIs) and avoided crossing regions in the photochemistry of this motor (and related compounds)? Can the photostationary state of **1**, in which the ratio of the concentrations of the stable conformer **1-P** to the metastable conformer **1-M** is 1:3,[15] be modified in a predictable manner? In determining the relative contribution of CIs and avoided crossings, what implications does the electronic structure of **1** have for the design of molecular motors? These questions will be addressed in a combined quantum chemical and molecular dynamics study of the operation cycle of the motor **1**, in which quantum chemistry is used to describe the energy landscape and molecular dynamics to use this landscape to predict empirically observed properties.

Currently, it is widely accepted that CI points or seams play a crucial role for the photochemistry of molecules as they represent funnels for highly efficient radiationless relaxation.[25] With the advent of ultrafast optical spectroscopic methods[26] it has become apparent that the excited states of molecules undergo transformation and radiationless relaxation to the ground state on too fast a time scale to be described in terms of the nonadiabatic coupling in the avoided crossing regions alone.[25] The role of CIs in molecular photochemistry and for predicting the direction of molecular photorearrangements has been recognized since the pioneering work of Yarkony[23] and Robb.[24] A clear example is the understanding of the photochemistry of small organic alkenes, such as ethylene, for which CIs occur upon pyramidalization of one of the carbon atoms accompanied by a twist about the double bond. This plays a crucial role in the course of the photorearrangement of ethylene, stilbene, etc.[25,27−29]

Thus, in the present study, the dynamics behind the photoisomerization of **1** are explored employing a balanced description of the avoided crossing regions and the regions where CI points or seams occur. Although such a description can be provided reliably by high level multireference ab initio methods, the application of these methods to fluorene-based molecules, and indeed many other molecular motors, is restricted by the sheer size of these molecules. Therefore, in this work, we employ a novel computational scheme[30,31] based on the ensemble approach[32−34] within density functional theory (DFT).[35] This approach is capable of providing a reliable description of the ground and excited states of molecular systems in which processes of bond breaking and bond formation occur based on comparison with empirical data.[30,31,34,36−40] This computational scheme will be applied in the present study to understand the ground and excited state PESs of **1** along the internal coordinates describing the twisting motion about the central double bond and pyramidalization of one of the adjacent carbon atoms. On the basis of the computational results, the geometric distortions necessary for **1** to reach the CIs will be analyzed, and a sequence of geometric transformations that the molecular motor undergoes during its photochemical isomerization will be constructed. The data obtained for the ground and excited state potential energy profiles will be used to parametrize a suitable force field for molecular dynamics simulations,[42] and the dynamics of photorearrangement are thereby studied. The results of the theoretical calculations are considered in the context of the experimentally observed photostationary state of **1**[15] and of the results of a recent ultrafast transient absorption study of the excited state dynamics of molecules related to **1**.[41] The theoretical results obtained hold considerable implications in achieving a rational synthetic design of future molecular motors with application defined functionality.

SCHEME 2: Atom Numbering Scheme and Definition of Dihedral Angles in 1

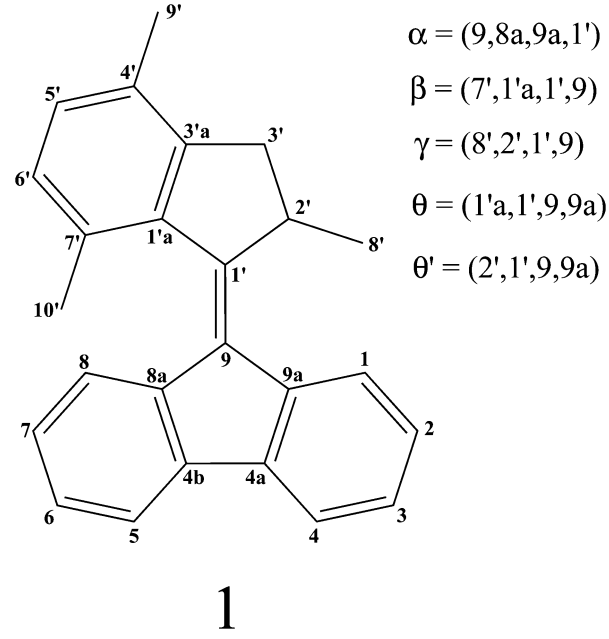

1

Results and Discussion

The operation cycle of fluorene motor **1** consists of four steps: two photoisomerization steps (power strokes), of which only one is shown in Scheme 1, and two thermally activated helix inversion steps.[15] The theoretical study begins with the investigation of the ground state PES of the first semicycle of **1** as shown in Scheme 1. Note that, in the ground state of **1**, breaking of the central double C═C bond occurs en route from the stable conformer **1-P** to the metastable conformer **1-M**. The purpose of this part of the study is to evaluate the kinetic stability of the conformers during the operation cycle of motor **1**. The next stage of the study addresses the excited state PES of the **1-P** → **1-M** photoisomerization in the regions of avoided crossing of the ground and excited state PESs and near possible CI points or seams. The ground and excited state PESs were scanned along the twisting and pyramidalization modes and the surfaces obtained were used in molecular dynamics simulations. Throughout this work the atomic numbering and the geometric parameters of **1**, which are shown in Scheme 2, are employed.

Ground State PES of the Fluorene Rotary Motor 1. The ground S_0 state PES of fluorene motor **1** was studied using B3LYP[43−45] calculations with the 6-31G* basis set[46] and together with the semiempirical PM3 method.[47] First, the stable conformations of **1** were optimized with the PM3 method and then reoptimized with the B3LYP method. Fluorene motor **1** features two minima in the ground state: the stable conformer **1-P**, in which the methyl group in 2 position adopts the axial orientation, and the metastable conformer **1-M**, in which the methyl group in the 2′ position is in equatorial orientation with respect to the ring axis (see Scheme 2). Note that the two identical stable conformers in Scheme 1 are denoted as **1-P** and **1-P′** to distinguish between the starting orientation of the motor and its orientation after the first half loop. The **1-M** conformer is less stable than **1-P** by 3.45 kcal/mol according to the B3LYP calculations. The most important geometry parameters and relative energies of the two conformers are listed in Table 1.

TABLE 1: Geometry Parameters (see Scheme 2 for Definitions) and Relative Electronic Energies of the 1-P and 1-M Conformations Obtained with the B3LYP/6-31G* Method and with the PM3 Semiempirical Method

	1-P		1-M		1-P′	
parameter	B3LYP	PM3	B3LYP	PM3	B3LYP	PM3
α (°)	1.7	1.7	1.6	1.0	−1.7	−1.7
β (°)	−43.1	−41.0	30.2	22.4	−43.1	−41.0
γ (°)	105.5	98.6	32.3	48.9	105.5	98.6
θ (°)	169.2	168.9	31.5	29.2	−15.6	−15.4
θ' (°)	−22.6	−23.2	−143.4	−147.2	153.0	152.5
$\mathbf{R}_{C_9C_{1'}}$ (Å)	1.368	1.349	1.376	1.354	1.368	1.349
ΔE (kcal/mol)	0	0	3.45	2.43	0	0

The S_0 PES for the thermal helix inversion step **1-M → 1-P′** (second stroke in the operation cycle of **1**, Scheme 1) was first scanned with the PM3 method along the dihedral angles θ (twist about the C_9—$C_{1'}$ double bond) and β (see Scheme 2 for definitions). According to the calculations, it is these angles that undergo the greatest variation during the thermal helix inversion step **1-M → 1-P′** (see Table 1). All other geometry variables were optimized during the scan. The ground state PES, which is shown in Figure 1, reveals that a transition state between the two structures is located at $\theta = 18.1°$ and $\beta = -32.2°$ according to the PM3 calculations. Using this geometry as the starting structure, a B3LYP/6-31G* search for transition state has been carried out, and the resulting structure ($\theta = 10.8°$ and $\beta = -25.4°$) was characterized by the vibrational analysis. A single imaginary vibrational frequency was found at the geometry of the transition state with all other frequencies real. The transition state found in the B3LYP/6-31G* calculation lies 22.1 kcal/mol higher than the **1-P′** conformer (see Scheme 3). Thus, the activation energy $\Delta^{\ddagger}E$ for the **1-M → 1-P′** transition is 18.7 kcal/mol, which upon correction for the thermal free energy yields $\Delta^{\ddagger}G° = 20.0$ kcal/mol. This activation free energy agrees reasonably well with the experimentally estimated $\Delta^{\ddagger}G°$ of 18.9 kcal/mol.[15]

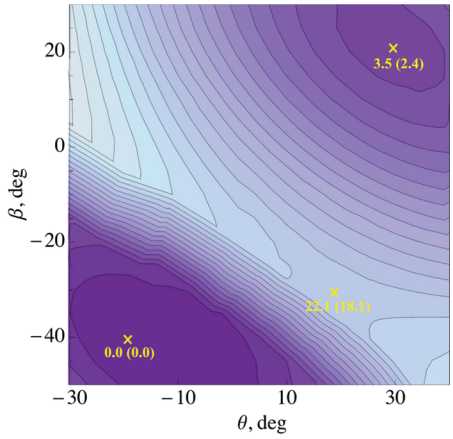

Figure 1. Ground state potential energy surface of the thermal helix inversion step. B3LYP/6-31G* energies outside parentheses, PM3 energies in parentheses.

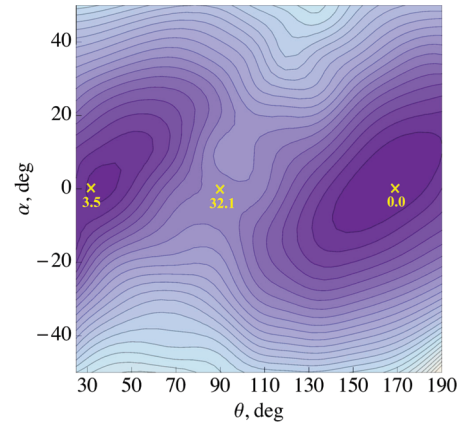

Figure 2. Ground state potential energy surface of the photoisomerization step as obtained with the RE-B3LYP/6-31G* method.

The ground state PES of the **1-P → 1-M** step (first stroke in the operation cycle of **1**, Scheme 1) involves breaking of the C_9═$C_{1'}$ double bond, and reliable modeling of this process requires a theoretical method capable of describing strong nondynamic electron correlations resulting from avoided crossing of the ground and the doubly excited electronic states near 90° of twist. Thus, the spin-restricted ensemble-referenced Kohn−Sham (REKS) method was employed in this work that has proved to be capable of reliably describing electronic states typified by the strong electron correlation.[34,36−40]

For the photoisomerization step **1-P → 1-M**, the ground state PES obtained in the RE-B3LYP/6-31G* calculations is shown in Figure 2. This PES was scanned along the twisting angle θ and pyramidalization angle α (see Scheme 2) with all other geometric parameters fully optimized. This was done for the subsequent modeling of the excited state PES and for the identification of regions where CIs may occur. The dihedral

SCHEME 3: Profiles of the Ground (S_0) and the Lowest Singlet Excited (S_1) State Potential Energy Surfaces of 1 along the Minimal Energy Path Connecting the Stable (P) and the Metastable (M) Isomers

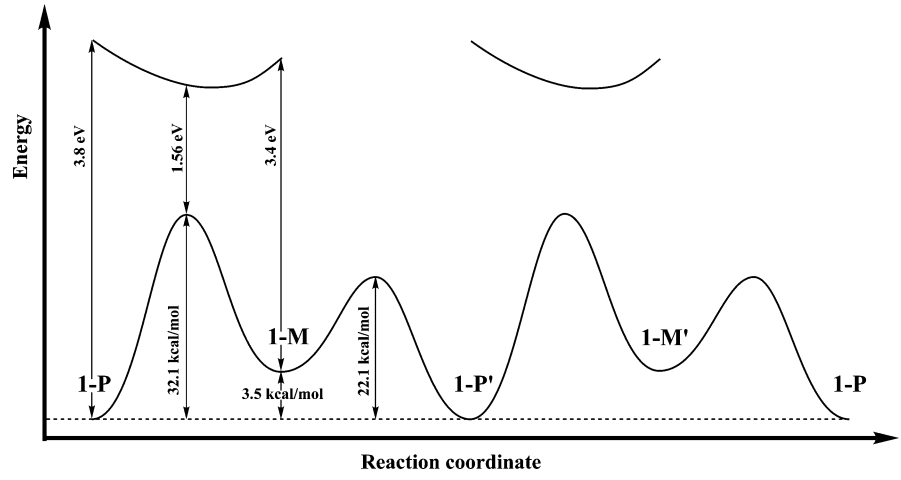

TABLE 2: Excitation Energies, in eV and in nm (in Parentheses), of the Stable Conformers 1-P and 1-M Calculated with the SA-REBH&HLYP and TD-BH&HLYP Methods

	SA-REBH&HLYP		TD-BH&HLYP	
basis set	**1-P**	**1-M**	**1-P**	**1-M**
6-31G*	3.80 (327)	3.40 (365)	3.78 (328)	3.39 (366)
6-311G**	3.74 (331)	3.34 (371)	3.72 (333)	3.32 (373)
6-311+G**	3.71 (334)	3.31 (375)	3.68 (337)	3.28 (378)

angle α characterizes pyramidalization of the atom C_9, and it was selected for the scan because reaching a CI between the S_0 and S_1 PESs in alkenes requires both a twist about the double bond and pyramidalization of one of the adjacent carbon atoms.[23−25,29] It is noteworthy that pyramidalization of the $C_{1'}$ carbon did not lead to occurrence of CI points as was established in the ground and the lowest excited singlet state calculations (see below). Because we are interested in locating CIs between these states, we did not pursue the $C_{1'}$ pyramidalization in the PES scans.

The ground state PES of the **1-P** → **1-M** step features a transition state at $\theta = 91°$ and $\alpha = 1°$, which lies 32.1 kcal/mol above the stable conformer **1-P** as shown in Figure 2 and in Scheme 3. Thus, there is a substantial energy difference between the barrier heights of the **1-P** → **1-M** and the **1-M** → **1-P′** steps, which implies that the back transformation **1-M** → **1-P** via twist about the C_9═$C_{1'}$ double bond is very unlikely and the thermal isomerization occurs in the direction **1-M** → **1-P′** via an inversion of helicity.

Excited State PES of the Fluorene Rotary Motor 1. The lowest singlet excited states of the **1-P** and **1-M** conformers were studied with the TD-BH&HLYP/6-31G* method. In these calculations, the geometries of **1-P** and **1-M** were taken from the B3LYP/6-31G* calculations. These calculations revealed that the lowest singlet excited state corresponds to the excitation of a single electron from the π -bonding to the π -antibonding orbital of the C_9═$C_{1'}$ double bond. The calculated oscillator strenght of the $S_0 \rightarrow S_1$ excitation is 0.63 in the **1-P** conformer and 0.59 in the **1-M** conformer. The next four transitions have oscillator strenghts below 0.05, and the next significant absorption band is to a state 1.6 eV above the S_1 state. Thus, the S_1 state, which has zwitterionic character and through which the **1-P** → **1-M** photoisomerization occurs, is optically accessible. As there are no other signlet excited states below S_1, it is sufficient to consider only this state in the analysis of the **1-P** → **1-M** photoisomerization. Note that this is different from the widely accepted models that consider transitions between two (or more) excited states at the early stage of photisomerization of molecules related to **1**, for example, stilbene.[48]

The S_1 state of **1** was studied with the use of the state averaged REKS (SA-REKS) method, because this method is capable of describing excitation energies of molecules in regions where strong nondynamic electron correlation dominates the electronic structure, such as in avoided crossing regions.[30,31,49] It is important to note that the more widely used time-dependent DFT (TD-DFT) methods[50] can not yield reliable excitation energies in these regions.[30] The $S_0 \rightarrow S_1$ excitation energies of the **1-P** and **1-M** conformers obtained using the SA-REBH&HLYP method and the TD-BH&HLYP method using the 6-31G*, 6-311G**, and 6-311+G** basis sets[46] are listed in Table 2. Experimentally measured maxima of major absorption bands of the **1-P** and **1-M** conformers in hexane at −40 °C are 360 and 385 nm, respectively.[15] Considering that environmental effects and the vibrational corrections to the excitation energies were not taken into account in the calculations, the agreement with the experimental data is good. There is also a good agreement between the TD-BH&HLYP calculations and the SA-REKS calculations. The time-dependent formalism, however, is not applicable in the avoided crossing region, near $\theta = 90°$, where breaking of the C_9═$C_{1'}$ double bond occurs, whereas the SA-REKS method is capable of reliably describing the lowest excited states of molecular systems with broken bonds.[30,31]

The ground S_0 and the excited S_1 state PESs obtained in the SA-REBH&HLYP/6-31G* calculations are shown in Figure 3.[51] The S_0 and S_1 PESs were calculated using the geometries optimized in the RE-B3LYP/6-31G* calculations for the ground state (see above). For comparison, the TD-BH&HLYP/6-31G* calculations were carried out at a number of points on the $\theta-\alpha$ grid. In the regions near the local minima on the ground state PES there is a good agreement between the two methods, similar to that reported in Table 2. However, in the region $80° \le \theta \le 110°$ and $-30° \le \alpha \le 30°$, where there is an avoided crossing of the two PESs, the TD-DFT formalism fails.[30] In the ground S_0 state, the $(...\pi^2\pi^{*0})$ and $(...\pi^0\pi^{*2})$ electronic configurations become (nearly) degenerate, and this leads to a break down of computational methods based on the single reference description of the ground state.[33,34] The REKS method can be used in these cases, because it provides a multireference description of

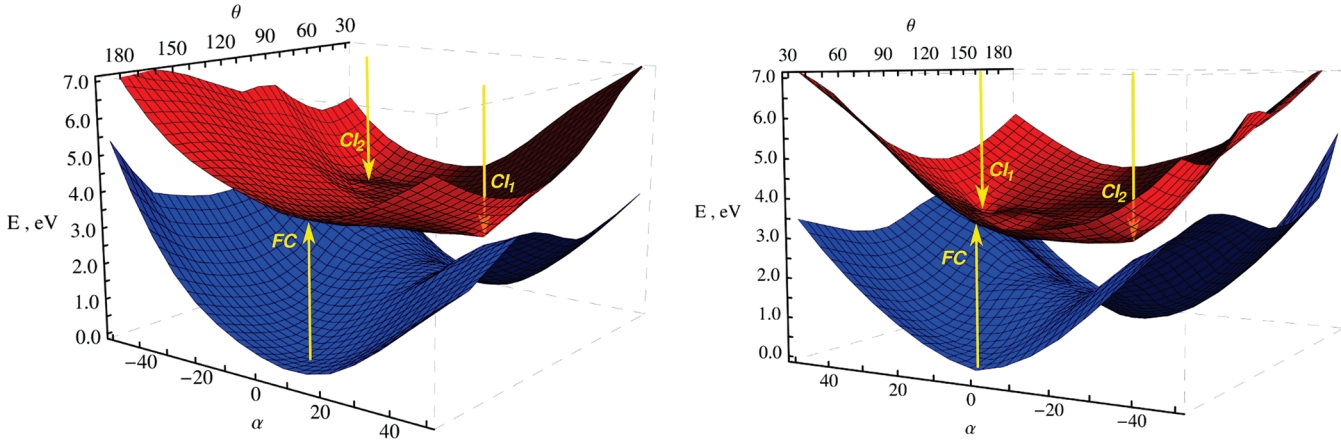

Figure 3. Profiles of the S_0 (blue) and S_1 (red) PESs of **1** obtained in SA-REBH&HLYP/6-31G* calculations (see text for details). Left panel: view from the side of the **1-P** conformation. Right panel: view from the side of the **1-M** conformation. Positions of the Franck−Condon points and conical intersections are shown with yellow arrows.

nondynamic electron correlation by adopting fractional occupation numbers of the frontier orbitals.[34,36−40]

Near the transition state on the ground state PES ($\theta = 91°$ and $\alpha = 1°$) the energy gap between the S_0 and S_1 states as obtained in the SA-REBH&HLYP/6-31G* calculation amounts to 1.56 eV. With increase in the angle α, the gap between the surfaces narrows down and at $\alpha = 34°$ and $\theta = 120°$ it becomes 0.16 eV (3.7 kcal/mol). This small value indicates the presence of CI near this geometry.[52] Because analytic energy gradients are not yet implemented in the SA-REKS formalism, we did not attempt to optimize a minimal energy CI (MECI) point.[53] However, population transfer from the excited S_1 state to the ground S_0 state occurs via a funnel in which the whole manifold of CI points plays an important role, especially the CIs closest to the Franck−Condon point.[25,29] The CI point identified in the S_0−S_1 PESs scan indicates that to reach this funnel a simultaneous twist about the double bond and a substantial pyramidalization of the C_9 atom are necessary. This is consistent with the results obtained for simple alkenes, such as ethylene or butadiene,[27,25,29] and for stilbene.[27] Note that the pyramidalization angle of the atom C_9 (i.e., the angle between the C_9−C_{8a}−C_{9a} plane and the C_9−$C_{1'}$ bond) obtained for the CI point of **1** is 52. 7°, which is close to the pyramidalization angle of 58. 8° obtained by Levine et al.[29] in the CASPT2 calculations on ethylene.

The CI point at $\alpha = 34°$ and $\theta = 120°$ lies ca. 3 eV above the ground state energy of the **1-P** conformer and ca. 0.7 eV below the Franck−Condon point. As can be seen in Figure 3, this CI has peaked topography, which implies that reaching the crossing seam on the S_1 surface should proceed without delays.[25] This observation is consistent with the results of the ultrafast transient absorption study of molecular motors by Augulis et al.[41] who found that on average the molecule spends ca. 1.7 ps in the excited state. Note that the CI point corresponds to a local minimum on the S_1 PES that can be reached easily from the Franck−Condon region (near the **1-P** geometry). Thus, the decay to the ground state occurs as an essentially barrierless process[25] that is consistent with the short excited state decay time observed experimentally.

In addition to the CI point at $\alpha = 34°$ and $\theta = 120°$ (CI_1), the onset of another CI point was observed at $\alpha = -28°$ and $\theta = 64°$ (CI_2). Indeed, if in a molecule with reflection symmetry, such as ethylene, there would be two CI points on opposite sides of the avoided crossing region and related by mirror symmetry. In a chiral molecule, such as the fluorene motor **1**, the two CI points can not be precise mirror images of one another, however both occur on opposite sides of the avoided crossing region. In our calculations, the CI_2 structure could not be precisely located on the grid chosen for the PES scans; the energy gap at $\alpha = -28°$ and $\theta = 64°$ is 0.16 eV, and this structure lies ca. 0.5 eV lower in energy than the nearest Franck−Condon point (**1-M** conformer). Although the CI_2 structure can in principle be reached upon excitation from both conformers, the molecular dynamics simulations described in the subsequent section reveal that the majority of the trajectories on the S_1 PES started in the **1-P** conformer pass near the CI_1 structure, whereas the CI_2 point plays a minor role in the dynamics of the motor. Therefore, CI_1 can be considered as a more important mechanistic feature in the **1-P** → **1-M** photoisomerization and in the following is referred to as **1-CI** for brevity.

Using the results of our calculations the full operation cycle of the fluorene motor **1** can be presented as shown in Scheme 4. The initial structure **1-P** undergoes photo excitation to the S_1 state upon which it relaxes via the conical intersection **1-CI** to the ground S_0 state. On the ground state PES, it undergoes rapid barrierless relaxation to the **1-M** conformer that then undergoes a thermal helix inversion step passing through the **1-TS** transition state ($\Delta^{\ddagger}E = 18.7$ kcal/mol). After that, the system arrives at the **1-P′** structure, which is the **1-P** conformer rotated through 180° about a line passing through the central double bond, and the system repeats the above steps starting from the **1-P′** conformer. This completes the full rotation cycle of the fluorene motor **1**. Of note, in a recent combined experimental and theoretical study on a molecular switch structurally close to **1**, a barrierless excited state reaction path leading to conical intersections was found by Sinicropi et al.[54] and Rivado-Casas et al.[55]

SCHEME 4: Full Rotation Cycle of Fluorene Motor 1

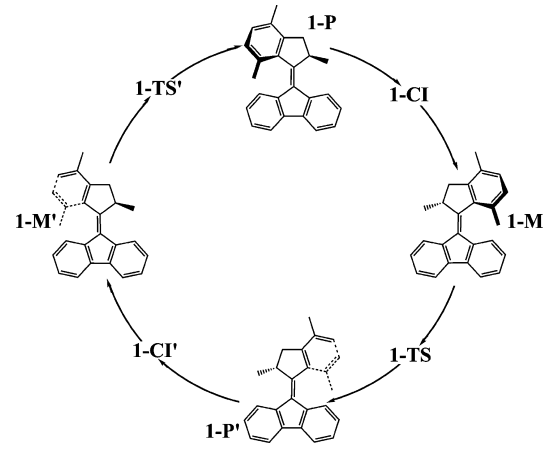

The molecular geometries of the **1-P**, **1-CI**, **1-M**, and **1-TS** structures are shown in Figure 4. It can be seen that en route to the **1-M** conformer, **1** undergoes strong pyramidalization of the C_9 atom (in the **1-CI** structure) that results in a substantial tilt of the rotating part of the molecule from the axis of rotation (the C_9−$C_{1'}$ double bond). Somewhat less of a deviation from the rotation axis occurs during the helix inversion step, where pyramidalization of both C_9 and $C_{1'}$ atoms occurs in the **1-TS** structure. Note, however, that in **1-TS** the upper part of the molecule tilts to the opposite side of the molecule than what occurs during the photoisomerization step. Thus, during the first half cycle in Scheme 4, the rotating part of the motor **1** carries out a combined tilt-twist motion that resembles the motion of a butterfly wing rather than a pure rotation.

These results also help to understand the dynamics of relaxation from the **1-CI** structure to the **1-M** conformer that proceeds on the ground state PES. Because there is a substantial difference in the tilting angle of the rotor in these structures, a noticeable excitation of the respective vibrational modes of **1-M** can be expected (these modes have frequencies of ca. 400 cm^{-1} according to the calculations). Vibrational cooling of the **1-M** is expected to occur within characteristic times of the order of 10−20 ps,[56] which is consistent with the experimental observations of Augulis et al.[41]

Molecular Dynamics Simulations. In the preceding section, the study of the S_0 and S_1 PESs was carried out for static molecular structures. It reveals a number of key features of the potential energy landscapes. The question remains however as to how important dynamic effects are for the photoisomerization? Can the quantum yields of photoisomerization when starting from the **1-P** or from the **1-M** conformer be understood? Hence, are we able to explain the photostationary state (PSS) observed experimentally? To address these questions and to obtain a more realistic theoretical description of light driven

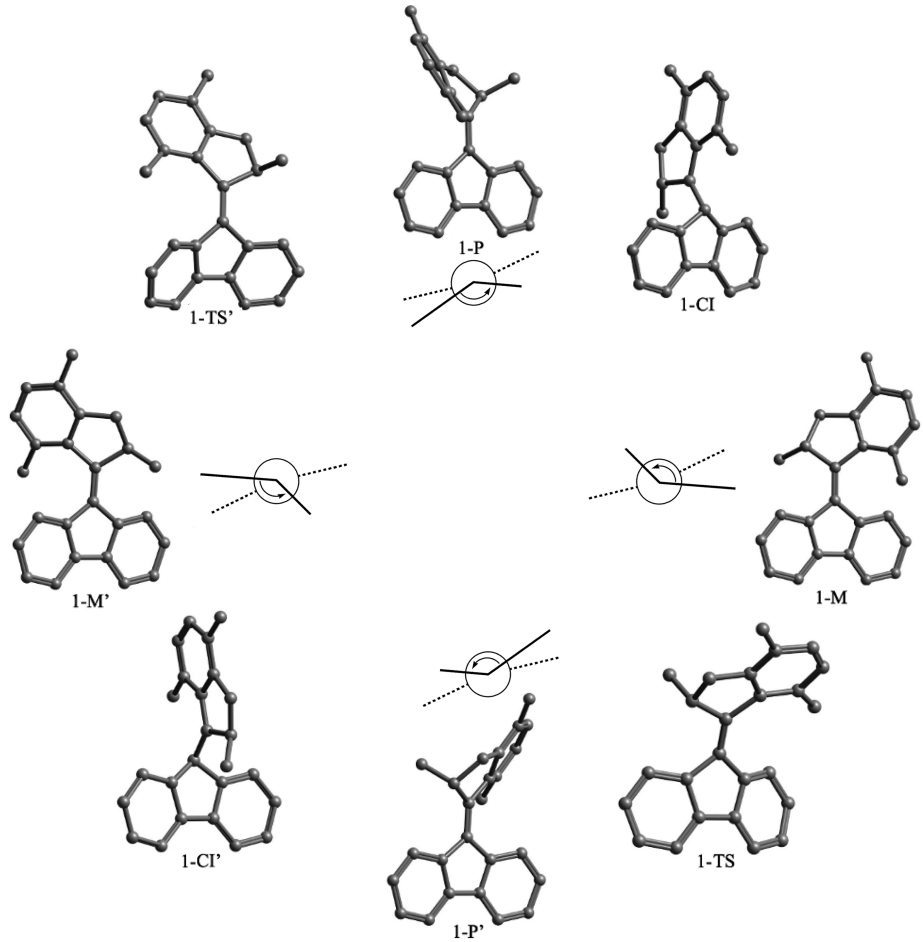

Figure 4. Geometries of the most important structures involved in the rotation cycle of fluorene motor **1** as obtained from our quantum chemical calculations. Hydrogen atoms were removed for clarity.

molecular motion we carried out molecular dynamics (MD) simulations based on the PESs of the ground and excited states obtained.

Excited state MD simulations[57] employing an on-the-fly quantum-chemical description of the PESs involved have been applied recently to a range of molecules, such as chromophores of photoreceptor proteins,[58−62] fluorescent proteins,[63−65] and (bacterio)rhodopsin,[66−70] as well as to DNA bases.[71−76] In these studies, wave function-based quantum-chemical methods, such as CASSCF and CASPT2, as well as density functional methods and semiempirical methods specifically adapted to describe avoided crossings and conical intersections in molecules were used. In a recent study of a first-generation molecular rotor,[77] a density functional method not suited for the description of bond breaking processes and avoided crossing regions was employed. In the vast majority of the cases, the large computational cost of the quantum-chemical calculations limited the accessible time and length scales of simulations, rendering it impossible to obtain a statistically significant number of trajectories. In the present case, the size of the molecular motor **1** prohibits a straightforward application of quantum-chemical methods to study the excited state dynamics. Thus, we resorted to the OPLS all-atom force field[78] as an efficient alternative, enabling us to run a large number of independent simulations. As detailed below, the statistics provided by this approach allows different possible photochemical reaction pathways to be distinguished.

The OPLS all-atom force field was parametrized against the S_0 and S_1 potential energy surfaces obtained from our REKS calculations, with a particular focus on the important torsion θ and pyramidalization α coordinates in setting up the MD simulations (for details, see the Supporting Information). The mean absolute errors of the S_0 and S_1 surfaces with respect to those obtained from our REKS calculations are on the order of 0.2 eV (4.6 kcal/mol), which is acceptable for our purposes. Furthermore, the OPLS and REKS surfaces (see Supporting Information) exhibit the same qualitative features: a barrierless rotation about the C_9—$C_{1'}$ bond (dihedral angle θ) and a minimum at nonzero pyramidalization (dihedral angle α) in the excited S_1 state, and a large energy barrier to C_9—$C_{1'}$ double bond rotation of ca. 37 kcal/mol in the ground S_0 state.

In the MD simulations, 100 trajectories were initiated from both the **1-P** conformer and the **1-M** conformer, respectively. The S_1 trajectories were initiated from snapshots taken from equilibrated ground state simulations. At time $t = 0$, the molecule is excited vertically to the S_1 state where it evolves freely until it reaches a region where surface hopping occurs. After the surface hop back to the ground S_0 state, the molecule relaxes toward one of the conformers, **1-P** or **1-M**. According to the Landau−Zener formula,[80] the probability of the surface hop, P_{hop}, depends exponentially on the magnitude of the energy gap ΔE between the PESs, $P_{hop} = \exp[-(\pi\Delta E)/(4\hbar D)]$ (D is the nonadiabatic coupling between the two states). Thus, P_{hop} reaches a maximum at or near the CI seams ($\Delta E = 0$). Here we adopted an assumption that surface hopping occurs exclusively at the CI.[71] The root-mean-square deviation (rmsd) of the coordinates of heavy atoms from the CI structures obtained in the SA-REBH&HLYP calculations was used as a criterion of proximity to the CI. As soon as the heavy-atom rmsd dropped

TABLE 3: Excited State Decay Times τ_{S_1} and Quantum Yields ϕ_{iso} of Photoisomerization Obtained from MD Simulations[a]

	1-P conformer	**1-M** conformer
τ_{S_1} (ps)	1.40 ± 0.10	1.77 ± 0.13
ϕ_{iso} (%)	92	40
SH[b] at CI_1 (%)	63	49
SH at CI_2 (%)	37	51
ϕ_{iso, CI_1}[c] (%)	98	37
ϕ_{iso, CI_2} (%)	81	43

[a] 100 simulations were initiated from the **1-P** and **1-M** conformation, respectively. [b] SH: surface hop. [c] Quantum yield of photoisomerization at the respective CI point.

below a threshold of 0.32 Å during the S_1 dynamics, a surface hop back to S_0 was imposed (see Theoretical Methods section).

Table 3 summarizes the results of the MD simulations. All excited state trajectories sample structural regions close to CI_1 (with $\alpha = 34°$ and $\theta = 120°$) or CI_2 (with $\alpha = -28°$ and $\theta = 64°$), and ultimately successfully hop to the ground state. In each trajectory, the time spent on S_1 was taken as the excited state lifetime. The individual S_1 lifetimes range from 0.66 to 6.31 ps and 0.17 to 5.92 ps in the simulations initiated in the **1-P** and **1-M** conformers, respectively. Fitting a single-exponential decay to the lifetimes observed in the simulations initiated in the **1-P** conformation yielded a respective ensemble decay time[79] $\tau_{S_1} = 1.40 \pm 0.10$ ps. Closer analysis of the lifetime distributions revealed that the simulations initiated in the **1-M** conformer follow a biexponential decay: In 15 out of 100 simulations, an excited state lifetime below 0.24 ps is observed (with an ensemble decay time of $\tau_{S_1} = 0.20 \pm 0.01$ ps), whereas the remaining 85 simulations exhibit a significantly slower S_1 decay, with $\tau_{S_1} = 1.77 \pm 0.13$ ps. These lifetimes agree with the excited state decay time of about 1.7 ps measured for a similar molecular motor.[41]

The quantum yields for the photoisomerizations initiated in the **1-P** and **1-M** conformers, respectively, are quite different (Table 3): whereas $\phi_{P\rightarrow M}$ is as large as 92%, the $\phi_{M\rightarrow P}$ is only 40%. Interestingly, all 15 simulations with an S_1 lifetime <0.24 ps successfully isomerize and thus significantly contribute to $\phi_{M\rightarrow P}$. Taken together, the ratio $\phi_{P\rightarrow M}/\phi_{M\rightarrow P}$ is ca. 2.3:1, which needs to be corrected for the ratio of optical absorption cross sections of both conformers to obtain the photostationary state ratio. At $\lambda = 365$ nm, the observed ratio of molar absorptivites of the **1-P** to **1-M** conformers is ca. 1.5:1.[15] Hence, the theoretical estimate for PSS is ca. 3.5:1, in excellent agreement with the experimental value of ca. 3:1.[15]

Next, we analyzed whether a certain part of the S_1/S_0 intersection seam is predominantly accessed, and if so, whether the vicinity of CI_1 or CI_2 is preferred. Indeed, as shown in Table 3, S_1 decay predominantly occurs at CI_1, when starting from the **1-P** conformation. From the 100 simulations initiated in the **1-P** conformer, 63 decay at CI_1, and only 37 at CI_2. This behavior might have been expected due to the proximity of CI_1 to the Franck−Condon region of **1-P** (see Figure 3). For the trajectories initiated in the **1-M** conformer, the surface hop at CI_1 occurs at about the same frequency as at CI_2, despite that CI_1 is farther away from the **1-M** Franck−Condon region than CI_2. This result underlines the importance of the dynamics in the excited state process. In this context, it is crucial to run many independent simulations (here: 100) to be able to distinguish between different possible photochemical reaction pathways. Finally, we separately analyzed the isomerization quantum yields in the vicinity of the two CI structures. The

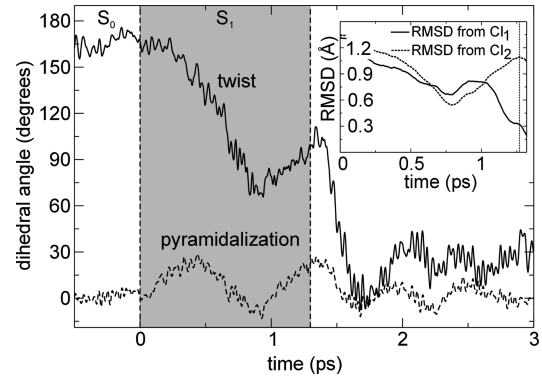

Figure 5. Time evolution of twist θ (solid line) and pyramidalization α (dashed line) during P-to-M photoisomerization trajectory. The gray-shaded area indicates evolution in the excited state S_1. The inset shows the heavy-atom rmsd from the CI_1 and CI_2 geometries during system evolution in the excited state; the surface hop is indicated by a dashed line (see text for detail).

analysis shows that the high $\phi_{P\rightarrow M}$ is due to a very high isomerization quantum yield of 98% at CI_1. Likewise, the lower value of $\phi_{M\rightarrow P}$ is also determined by the isomerization quantum yield at CI_1, which in this case is only 37%.

Figure 5 shows the time evolution of the twist and pyramidalization angle (θ and α, respectively) along a representative MD trajectory. The dynamics can be separated into three phases: (i) evolution on the ground state S_0, (ii) excitation and evolution on the excited state S_1, and (iii) decay back to S_0 at the CI and subsequent relaxation on the ground state surface. Within ca. 1 ps after excitation to S_1, rapid rotation about the $C_9{-}C_{1'}$ double bond (dihedral angle θ) occurs. However, this motion does not immediately lead to a surface hop, since the vibrational period of the pyramidalization motion (dihedral angle α) is faster: α adopted a value of about +30° already at around 0.4 ps, a time at which the rotor part of the molecule did not yet reach a fully perpendicular orientation with respect to the stator part due to its inertia. The CI seam is then accessed upon the second vibrational motion of the pyramidalization angle toward +30°, which occurs after about 1.3 ps (see inset in Figure 5). Subsequently, the molecule isomerizes to the M-conformation, a motion that is already completed after 1.6 ps. The final relaxation in the S_0 M-minimum is accompanied by a damped pyramidalization motion.

Taken together, the MD simulations provide a detailed picture of the structural dynamics that governs the photo conversion processes and support the conclusions based on the study of the topology of the ground and excited state PESs of **1**. The characteristic lifetimes of the excited state and the ratio of quantum yields of the two possible photoisomerizations (the photostationary state) nicely match and explain the experimentally observed data,[15,41] confirming the validity of the analysis of the photoisomerization mechanism undertaken in the present work.

Conclusions

In this contribution, the results of a combined quantum chemical and molecular dynamics study of the mechanism of the photoisomerization step of the rotational cycle of fluorene-based molecular rotary motor **1**[15] are reported. Unidirectional rotation in this motor is achieved due to the periodic repetition of photoisomerization and thermal relaxation steps. A high degree of control over the thermally activated helix inversion step was achieved that led to the formulation of clear design

principles for the thermal step in molecular rotary motors based on overcrowded alkenes.[13−15] Hitherto, the photoisomerization step remained poorly understood and less subject to rational design based on a firm understanding of the underlying principles. The study reported in this contribution is a first step toward unraveling these principles and toward formulating the rules for the improved design of photoisomerization steps and molecular motors in general.

The analysis of the ground and lowest singlet excited state PESs obtained in quantum chemical calculations reveals that conical intersections[23−25] play a central role in the mechanism of photo conversion between the stable **1-P** conformer and the metastable **1-M** conformer. Although, in this study, we focus on the zwitterionic singlet excited state,[51] the obtained results provide ample evidence that the photoisomerization of **1** occurs via a mechanism similar to ethylene and stilbene.[25,27,29] Low energy points on the CI seam are reached through a combined twist-pyramidalization motion of the rotor part of **1**, thus leading to a substantial tilt of the rotor from the axis of rotation. Molecular dynamics simulations carried out for both possible photoisomerization reactions, **1-P** → **1-M** and **1-M** → **1-P**, predict different quantum yields of isomerization, $\phi_{P\rightarrow M} = 0.92$ and $\phi_{M\rightarrow P} = 0.40$, which upon correction for the spectral overlap explain the occurrence of a photostationary state with the experimentally measured ratio of ca. 3:1 of the concentrations of the metastable and stable conformers.[15] Because conical intersections govern the photostationary state, rational synthetic design of the photoisomerization step should be directed toward controlling the regions where CIs occur. In this respect, theoretical study of the factors dominating the electronic structure in the CI seams and avoided crossing regions can provide a crucial piece of information complementing experimental studies. For example, it is expected that flattening the rotor and the stator geometries (that is, making them less pyramidalized) at the CI points as a result of substitution/chemical modification may lead to a different dynamics and, as a consequence, to a different photostationary state.

Interestingly, molecular dynamics simulations of the excited state dynamics of **1** indicate that the excited states may show multimodal decay patterns. Whereas for the **1-P** → **1-M** photoisomerization reaction a single-exponential decay with the average excited state lifetime of $\tau_{S_1} = 1.40 \pm 0.10$ ps was found in the simulations, the reverse photoisomerization, **1-M** → **1-P**, shows a biexponential decay with the lifetimes of $\tau_{S_1} = 0.20 \pm 0.01$ ps and $\tau_{S_1} = 1.77 \pm 0.13$ ps. This observation offers an alternative explanation to the transient absorption experiments where different decay times were interpreted in terms of a multistate model as resulting from transitions between several excited states.[41,48,87] Indeed, if, on the excited state surface, the system can follow several trajectories with distinct lifetimes, the interpretation of the experimentally observed multiexponential decay times can be achieved in terms of two states only: the ground state and the lowest excited state. This conjecture will be verified experimentally in future studies where information provided by solvent effects and the effects of substitution on the observed photostationary state will be investigated.

Theoretical Methods

The ground state PES of the motor **1** was studied using the B3LYP density functional.[43−45] The Gaussian 03 quantum chemical program[83] was used in these calculations. In the calculations on the first step of the operation cycle of **1** (see Scheme 1), during which breaking of the central C_9—$C_{1'}$ double bond occurs, the spin-restricted ensemble-referenced Kohn−Sham (REKS) method[34,36−40] was used in combination with the B3LYP functional. The REKS method is capable of correctly describing the systems where avoided crossing of the PESs occurs due to near degeneracy of several electronic configurations, such as molecules with broken bonds. In the ground state calculations, the 6-31G* basis set[46] was employed on all atoms. The REKS and SA-REKS calculations were carried out with the use of the Cologne08 code.[84]

The excitation energies and the lowest singlet excited state PES of **1** were calculated with the use of a recently developed state-averaged (SA) variant of the REKS method.[30,31] In these calculations the BH&HLYP density functional was employed, because it provides for a better compensation of the self-interaction error of the approximate density functional,[85] which is important for the SA-REKS calculations.[30,31] The functionals with increased fraction of the exact exchange, such as the BH&HLYP density functional, are capable of accurately describing the excited states with electron transfer character[86] and provide balanced description of the zwitterionic excited states within the SA-REKS formalism.[30,31] In the SA-REKS calculations, the molecular geometries obtained in the ground state PES scans with the RE-B3LYP/6-31G* method were used in combination with the basis sets of varying size ranging from 6 to 31G* to 6-311+G**. A coarse grid with an increment of 10° for dihedral angles was used in these scans that was supplemented with a finer grid with an increment of 1° in the vicinity of conical intersections. For comparison, the TD-DFT calculations with the BH&HLYP functional were carried out for the geometries in proximity of the **1-P** and **1-M** conformers.

The MD simulations were carried out with the Gromacs (v4.0.5) program package.[81] The OPLS all-atom force field[78] was used, with the parametrization of the excited state PES as described in this work. A 1 fs time step was used to integrate the equations of motion, since no constraints were applied to the bonds and angles. No cutoffs were used for the nonbonded interactions.

All MD simulations in the excited state were initiated from equally spaced snapshots taken from a 1 ns ground state simulation that was equilibrated at −40 °C (temperature at which the PSS was experimentally measured) using velocity rescaling temperature coupling according to Bussi et al.[82] with a coupling time constant of 0.1 ps. As expected from the large energy barriers on S_0 for double bond isomerization and helix inversion, the molecule stayed in the starting conformation during the ground state equilibration. During the subsequent simulations, in which the system was first propagated on S_1 and, after the surface hop, evolved on the S_0 surface, no temperature coupling was applied.

In this work, a surface hopping procedure similar in spirit to the approach of Groenhof et al.[71] was followed. A surface hop back to the ground state occurred as soon as the molecule reached the vicinity of the CI seam. The heavy-atom coordinates rmsd from the quantum chemically obtained geometries of the CI_1 and CI_2 points was followed during the S_1 dynamics. A surface hop was imposed as soon as the rmsd to any of the two CI structures dropped below a certain threshold value. This threshold was chosen such that differences between the structures obtained with the force field and the quantum chemical calculations as well as finite-temperature effects are taken into account. To that end, we calculated the heavy-atom rmsd during the equilibrium 1 ns ground state force field MD simulation in the **1-P** conformation with respect to the quantum chemically optimized geometry, which yielded $\langle \text{rmsd} \rangle = 0.2$ Å with a standard deviation of $\sigma = 0.06$ Å. Finally, an rmsd-threshold

of 0.32 Å, as defined by adding 2σ to ⟨rmsd⟩, was used in the MD simulations.

Acknowledgment. L.V.S. thanks Andrzej Rzepiela for help with tabulated potentials in Gromacs, and The Netherlands Organisation for Scientific Research (NWO) for funding (Veni grant 700.57.404). B.L.F. and W.R.B. thank the Nanoned initiative, and W.R.B. thanks the NWO for funding (Vidi grant 700.57.42).

Supporting Information Available: This material is available free of charge via the Internet at http://pubs.acs.org.

References and Notes

(1) Stoddart, J. F. *Acc. Chem. Res.* **2001**, *34*, 410–411.
(2) Kottas, G. S.; Clarke, L. I.; Horinek, D.; Michl, J. *Chem. Rev.* **2005**, *105*, 1281–1376.
(3) Balzani, V.; Venturi, M.; Credi, A., *Molecular Devices and Machines, a Journey into the Nanoworld*; Wiley VCH: Weinheim, 2003.
(4) Feringa, B. L. *Acc. Chem. Res.* **2001**, *34*, 504–513.
(5) Feringa, B. L., Ed., *Molecular Switches*; Wiley-VCH: Weinheim, Germany, 2001.
(6) Browne, W. R.; Feringa, B. L. *Nat. Nanotechnol.* **2006**, *1*, 25–35.
(7) Feringa, B. L. *J. Org. Chem.* **2007**, *72*, 6635–6652.
(8) Comstock, M. J; Levy, N.; Kirakosian, A.; Cho, J.; Lauterwasser, F.; Harvey, J. H.; Strubbe, D. A.; Fréchet, J. M. J.; Trauner, D.; Louie, S. G.; Crommie, M. F. *Phys. Rev. Lett.* **2007**, *99*, 038301+.
(9) Kay, E. R.; Leigh, D. A.; Zerbetto, F. *Angew. Chem., Int. Ed.* **2007**, *46*, 72–191.
(10) Irie, M. *Bull. Chem. Soc. Jpn.* **2008**, *81*, 917–926.
(11) Balzani, V.; Credi, A.; Venturi, M. *Chem. Soc. Rev.* **2009**, *38*, 1542–1550.
(12) Koumura, N.; Zijlstra, R. W. J.; van Delden, R. A.; Harada, N.; Feringa, B. L. *Nature* **1999**, *401*, 152–155.
(13) Koumura, N.; Geertsema, E. M.; van Gelder, M. B.; Meetsma, A.; Feringa, B. L. *J. Am. Chem. Soc.* **2002**, *124*, 5037–5051.
(14) Pijper, D.; van Delden, R. A.; Meetsma, A.; Feringa, B. L. *J. Am. Chem. Soc.* **2005**, *127*, 17612–17613.
(15) Pollard, M. M.; Meetsma, A.; Feringa, B. L. *Org. Biomol. Chem.* **2008**, *6*, 507–512.
(16) Pollard, M. M.; Wesenhagen, P. V.; Pijper, D.; Feringa, B. L. *Org. Biomol. Chem.* **2008**, *6*, 1605–1612.
(17) Klok, M.; Boyle, N.; Pryce, M. T.; Meetsma, A.; Browne, W. R.; Feringa, B. L. *J. Am. Chem. Soc.* **2008**, *130*, 10484–10485.
(18) van Delden, R. A.; ter Wiel, M. K. J.; Pollard, M. M.; Vicario, J.; Koumura, N.; Feringa, B. L. *Nature* **2005**, *437*, 1337–1340.
(19) London, G.; Carroll, G. T.; Fernández Landaluce, T.; Pollard, M. M.; Rudolf, P.; Feringa, B. L. *Chem. Commun.* **2009**, 1712–1714.
(20) Browne, W. R.; Feringa, B. L. *Annu. Rev. Phys. Chem.* **2009**, *60*, 407–428.
(21) Geertsma, E. M.; van der Molen, S. J.; Martens, M.; Feringa, B. L. *Proc. Natl. Acad. Sci.* **2009**, *106*, 16919–16924.
(22) Klok, M.; Janssen, L. P. B. M.; Browne, W. R.; Feringa, B. L. *Faraday Discuss.* **2009**, *143*, 319–334.
(23) Yarkony, D. R. *Rev. Mod. Phys.* **1996**, *68*, 985–1013.
(24) Bernardi, F.; Olivucci, M.; Robb, M. A. *Chem. Soc. Rev.* **1996**, *25*, 321–328.
(25) Levine, B. G.; Martinez, T. J. *Annu. Rev. Phys. Chem.* **2007**, *58*, 613–634.
(26) Zewail, A. H. *J. Phys. Chem. A* **2000**, *104*, 5660–5694, and references cited therein.
(27) Quenneville, J.; Martinez, T. J. *J. Phys. Chem. A* **2003**, *107*, 829–837.
(28) Schultz, T.; Quenneville, J.; Levine, B.; Toniolo, A.; Martinez, T. J.; Lochbrunner, S.; Schmitt, M.; Shaffer, J. P.; Zgierski, M. Z.; Stolow, A. *J. Am. Chem. Soc.* **2003**, *125*, 8098–8099.
(29) Levine, B. G.; Coe, J. D.; Martinez, T. J. *J. Phys. Chem. B* **2008**, *112*, 405–413.
(30) Kazaryan, A.; Heuver, J.; Filatov, M. *J. Phys. Chem. A* **2008**, *112*, 12980–12988.
(31) Kazaryan, A.; Filatov, M. *J. Phys. Chem. A* **2009**, *113*, 11630–11634.
(32) Lieb, E. H. *Int. J. Quantum Chem.* **1983**, *24*, 243–277.
(33) Schipper, P. R. T.; Gritsenko, O. V.; Baerends, E. J. *Theor. Chem. Acc.* **1998**, *99*, 329–343.
(34) Filatov, M.; Shaik, S. *Chem. Phys. Lett.* **1999**, *304*, 429–437.
(35) Hohenberg, P.; Kohn, W *Phys. Rev.* **1964**, *136*, B864–B871. Kohn, W.; Sham, L. J. *Phys. Rev.* **1965**, *140*, A1133–A1138.
(36) Filatov, M.; Shaik, S. *J. Phys. Chem. A* **1999**, *103*, 8885–8889.
(37) Filatov, M.; Shaik, S. *J. Phys. Chem. A* **2000**, *104*, 6628–6636.
(38) de Visser, S. P.; Filatov, M.; Shaik, S. *Phys. Chem. Chem. Phys.* **2000**, *2*, 5046–5048.
(39) Illas, F.; Moreira, I.; de, P. R.; Bofill, J. M.; Filatov, M. *Phys. Rev. B* **2004**, *70*, 132414+.
(40) Moreira, I. D. R.; Costa, R.; Filatov, M.; Illas, F. *J. Chem. Theory Comput.* **2007**, *3*, 764–774.
(41) Augulis, R.; Klok, M.; Feringa, B. L.; van Loosdrecht, P. H. M. *Phys. Stat. Sol., C* **2009**, *6*, 181–184.
(42) Alder, B. J.; Wainwright, T. E. *J. Chem. Phys.* **1957**, *27*, 1208–1209. Alder, B. J.; Wainwright, T. E. *J. Chem. Phys.* **1959**, *31*, 459–466. Rahman, A. *Phys. Rev.* **1964**, *136*, A405–A411. Stillinger, F. H.; Rahman, A. *J. Chem. Phys.* **1974**, *60*, 1545–1557.
(43) Stephens, P. J.; Devlin, F. J.; Chabalowski, C. F.; Frisch, M. J. *J. Phys. Chem.* **1994**, *98*, 11623–11627.
(44) Becke, A. D. *J. Chem. Phys.* **1993**, *98*, 1372–1377.
(45) Lee, C.; Yang, W.; Parr, R. G. *Phys. Rev. B* **1988**, *37*, 785–789.
(46) Krishnan, R.; Binkley, J. S.; Seeger, R.; Pople, J. A. *J. Chem. Phys.* **1980**, *72*, 650–654.
(47) Stewart, J. J. P. *J. Comput. Chem.* **1989**, *10*, 209–220. ibid., 1989, *10*, 221−264.
(48) Fuss, W.; Kosmidis, C.; Schmid, W. E.; Trushin, S. A. *Angew. Chem., Int. Ed.* **2004**, *43*, 4178–4182.
(49) Note that the SA-REKS method is a first principles computational scheme that does not include any empirical parameters. In our previous works, the method was tested against the experimental excitation energies and the results of high level ab initio calculations.
(50) Casida, M. In *Recent Advances in Density Functional Methods*; Chong, D. P., Ed.; World Scientific: Singapore, 1995; p 155.
(51) Note that the SA-REKS method is capable of describing the covalent doubly excited state with the leading electronic configuration ($.\pi^0\pi^{*2}$). However, these results are not reported here because this state lies above the zwitterionic S_1 state (the gap drops to ca. 0.05 eV only near $\theta = 90°$ and $\alpha = 0°$) and does not seem to play a role in the photochemistry of **1**. This can be explained by the asymmetry of **1**, which leads to some stabilization of the zwitterionic S_1 state with respect to the covalent doubly excited state in the avoided crossing region.
(52) Truhlar, D. G.; Mead, C. A. *Phys. Rev. A* **2003**, *68*, 032501+.
(53) Although the analytic energy gradients for the excited state are not yet available in the SA-REKS implementation, this does not affect the results of the molecular dynamics simulations carried out in this work with the use of the OPLS molecular force field for which the analytic energy gradients are easily available.
(54) Sinicropi, A.; Martin, E.; Ryazantsev, M.; Helbing, J.; Briand, J.; Sharma, D.; Léonard, J.; Haacke, S.; Cannizzo, A.; Chergui, M.; Zanirato, V.; Fusi, S.; Santoro, F.; Basosi, R.; Ferré, N.; Olivucci, M. *Proc. Nat. Acad. Sci.* **2008**, *105*, 17642–17647.
(55) Rivado-Casas, L.; Sampedro, D.; Campos, P. J.; Fusi, S.; Zanirato, V.; Olivucci, M. *J. Org. Chem.* **2009**, *74*, 4666–4674.
(56) Park, S.-M.; Nguyen, P. H.; Stock, G. *J. Chem. Phys.* **2009**, *131*, 184503.
(57) Groenhof, G.; Schäfer, L. V.; Boggio-Pasqua, M.; Robb, M. A., In *Handbook of Molecular Biophysics*; Bohr, H. G., Ed.; Wiley-VCH: Weinheim, 2009.
(58) Groenhof, G.; Bouxin-Cademartory, M.; Hess, B.; de Visser, S. P.; Berendsen, H. J. C.; Olivucci, M.; Mark, A. E.; Robb, M. A. *J. Am. Chem. Soc.* **2004**, *126*, 4228–4233.
(59) Groenhof, G.; Schäfer, L. V.; Boggio-Pasqua, M.; Grubmüller, H.; Robb, M. A. *J. Am. Chem. Soc.* **2008**, *130*, 3250–3251.
(60) Boggio-Pasqua, M.; Robb, M. A.; Groenhof, G. *J. Am. Chem. Soc.* **2009**, *131*, 13580–13581.
(61) Ko, C.; Levine, B.; Toniolo, A.; Manohar, L.; Olsen, S.; Werner, H. J.; Martinez, T. J. *J. Am. Chem. Soc.* **2003**, *125*, 12710–12711.
(62) Ko, C.; Virshup, A. M.; Martinez, T. J. *Chem. Phys. Lett.* **2008**, *460*, 272–277.
(63) Schäfer, L. V.; Groenhof, G.; Boggio-Pasqua, M.; Robb, M. A.; Grubmüller, H. *PLoS Comput. Biol.* **2008**, *4*, e1000034.
(64) Virshup, A. M.; Punwong, C.; Pogorelov, T. V.; Lindquist, B. A.; Ko, C.; Martinez, T. J. *J. Phys. Chem. B* **2009**, *113*, 3280–3291.
(65) Toniolo, A.; Olsen, S.; Manohar, L.; Martinez, T. J. *Faraday Discuss.* **2004**, *127*, 149–163.
(66) Warshel, A.; Chu, Z. T. *J. Phys. Chem. B* **2001**, *40*, 9857–9871.
(67) Hayashi, S.; Tajkhorshid, E.; Schulten, K. *Biophys. J.* **2003**, *85*, 1440–1449.
(68) Hayashi, S.; Tajkhorshid, E.; Schulten, K. *Biophys. J.* **2009**, *96*, 403–416.
(69) Frutos, L. M.; Andruniow, T.; Santoro, F.; Ferre, N.; Olivucci, M. *Proc. Natl. Acad. Sci. U.S.A.* **2007**, *104*, 7764–7769.
(70) Röhrig, U. F.; Guidoni, L.; Laio, A.; Franck, I.; Röthlisberger, U. *J. Am. Chem. Soc.* **2004**, *126*, 15328–15329.
(71) Groenhof, G.; Schäfer, L. V.; Boggio-Pasqua, M.; Goette, M.; Grubmüller, H.; Robb, M. A. *J. Am. Chem. Soc.* **2007**, *129*, 6812–6819.
(72) Fabiano, E.; Thiel, W. *J. Phys. Chem. A* **2008**, *112*, 6859–6863.

(73) Lan, Z. G.; Fabiano, E.; Thiel, W. *ChemPhysChem* **2009**, *10*, 1225–1229.

(74) Lan, Z. G.; Fabiano, E.; Thiel, W. *J. Phys. Chem. B* **2009**, *11*, 3548–3555.

(75) Markwick, P. R. L.; Doltsinis, N. L. *J. Chem. Phys.* **2007**, *126*, 175102+.

(76) Nieber, H.; Doltsinis, N. L. *Chem. Phys.* **2008**, *347* (1−3), 405–412.

(77) Grimm, S.; Bräuchle, C.; Franck, I. *ChemPhysChem* **2005**, *6*, 1943–1947.

(78) Jorgensen, W. L.; Tirado-Rives, J. *J. Am. Chem. Soc.* **1988**, *110*, 1657–1666.

(79) Lange, O. F.; Schäfer, L. V.; Grubmüller, H. *J. Comput. Chem.* **2006**, *27*, 1693–1702.

(80) Wittig, C. *J. Phys. Chem. B* **2005**, *109*, 8428–8430.

(81) Hess, B.; Kutzner, C.; van der Spoel, D.; Lindahl, E. *J. Chem. Theory Comput.* **2008**, *4*, 435–447.

(82) Bussi, G.; Donadino, D.; Parrinello, M. *J. Chem. Phys.* **2007**, *126*, 014101+.

(83) Frisch, M. J.; Trucks, G. W.; Schlegel, H. B.; Scuseria, G. E.; Robb, M. A.; Cheeseman, J. R.; Montgomery, J. A., Jr.; Vreven, T.; Kudin, K. N.; Burant, J. C.; Millam, J. M.; Iyengar, S. S.; Tomasi, J.; Barone, V.; Mennucci, B.; Cossi, M.; Scalmani, G.; Rega, N.; Petersson, G. A.; Nakatsuji, H.; Hada, M.; Ehara, M.; Toyota, K.; Fukuda, R.; Hasegawa, J.; Ishida, M.; Nakajima, T.; Honda, Y.; Kitao, O.; Nakai, H.; Klene, M.; Li, X.; Knox, J. E.; Hratchian, H. P.; Cross, J. B.; Bakken, V.; Adamo, C.; Jaramillo, J.; Gomperts, R.; Stratmann, R. E.; Yazyev, O.; Austin, A. J.; Cammi, R.; Pomelli, C.; Ochterski, J. W.; Ayala, P. Y.; Morokuma, K.; Voth, G. A.; Salvador, P.; Dannenberg, J. J.; Zakrzewski, V. G.; Dapprich, S.; Daniels, A. D.; Strain, M. C.; Farkas, O.; Malick, D. K.; Rabuck, A. D.; Raghavachari, K.; Foresman, J. B.; Ortiz, J. V.; Cui, Q.; Baboul, A. G.; Clifford, S.; Cioslowski, J.; Stefanov, B. B.; Liu, G.; Liashenko, A.; Piskorz, P.; Komaromi, I.; Martin, R. L.; Fox, D. J.; Keith, T.; Al-Laham, M. A.; Peng, C. Y.; Nanayakkara, A.; Challacombe, M.; Gill, P. M. W.; Johnson, B.; Chen, W.; Wong, M. W.; Gonzalez, C.; Pople, J. A. *GAUSSIAN 03*, Revision B2; Gaussian Inc.: Pittsburgh, PA, 2003.

(84) Kraka, E.; Gräfenstein, J.; Filatov, M.; Joo, H.; Izotov, D.; Gauss, J.; He, Y.; Wu, A.; Polo, V.; Olsson, L.; Konkoli, Z.; He, Z.; Cremer, D., *COLOGNE08*; University of the Pacific: Stocton CA, 2008.

(85) Cremer, D. *Mol. Phys.* **2001**, *99*, 1899–1940. Polo, V.; Kraka, E.; Cremer, D. *Mol. Phys.* **2002**, *100*, 1771–1790.

(86) Wu, C.; Tretiak, S.; Chernyak, V. Y. *Chem. Phys. Lett.* **2007**, *433*, 305–311.

(87) Fleming, G. R., *Chemical Applications of Ultrafast Spectroscopy*; Oxford University Press: Oxford, 1986; Ch 6, pp 124−235.

JP100609M